Journal of Atmospheric and Solar-Terrestrial Physics 73 (2011) 1747–1761

Contents lists available at ScienceDirect

Journal of Atmospheric and Solar-Terrestrial Physics

journal homepage: www.elsevier.com/locate/jastp

Altitude variation of aerosol properties over the Himalayan range inferred from spatial measurements

U.C. Dumka [a,b,*], K. Krishna Moorthy [c], S.N. Tripathi [d], P. Hegde [c], Ram Sagar [a]

[a] Aryabhatta Research Institute of Observational Sciences, Manora Peak, Nainital, India
[b] Center for Atmospheric and Oceanic Sciences, Indian Institute of Science, Bangalore 560012, India
[c] Space Physics Laboratory, Vikram Sarabhai Space Centre, Thiruvananthapuram 695022, India
[d] Department of Civil Engineering, Indian Institute of Technology, Kanpur 208016, India

ARTICLE INFO

Article history:
Received 27 June 2010
Received in revised form
26 March 2011
Accepted 1 April 2011
Available online 15 April 2011

Keywords:
Altitude profile
Mixing height
Heating rate
Central Himalayas
Absorption aerosol optical depth
Absorption Ångström exponent

ABSTRACT

Altitude variations of the mass concentration of black carbon, number concentration of composite aerosols are examined along with the columnar spectral aerosol optical depths using state of the art instruments and the Ångström parameters are inferred from the ground based measurements at several altitude levels, en route from Manora Peak, Nainital (~1950 m above mean sea level) to a low altitude station Haldwani (~330 m above mean sea level) at its foothill within an aerial distance of <10,000 m. The measurements were done during the winter months (November–February) of 2005, 2006 and 2007 under fair weather conditions. The results show a rapid decrease in all the measured parameters with increase in altitude, with >60% contribution to the AOD coming from the regions below ~1000 m. The Ångström wavelength exponent remained high in the well mixed region, and decreased above. The normalized AOD gradient was used to estimate aerosol mixing height, which was found to be in the altitude range 1000–1500 m, above which the particle concentrations are slowly varying as a function of altitude. The heating rate at the surface is found to be maximum but decreases sharply with increase in altitude. Analysis of the wavelength dependence of absorption aerosol optical depth (AAOD) showed that the aerosol absorption over the site is generally due to mixed aerosols.

© 2011 Elsevier Ltd. All rights reserved.

1. Introduction

The study of altitude profile of aerosol properties in the atmosphere is important for the modeling of the radiative effects as well as for the computations related to the study of atmospheric boundary layer (ABL) stability (Haywood and Ramaswamy, 1998; Satheesh, 2002; Tripathi et al., 2005a; Satheesh et al., 2006). The mesoscale boundary layer dynamics controls the properties of aerosols in the atmosphere (Parameswaran et al., 1998; Moorthy et al., 2004; Tripathi et al., 2005a, 2007; Niranjan et al., 2007). Although the aerosols have potential role in global and regional climate change (Satheesh and Ramanathan, 2000; Intergovernmental Panel on Climate Change, 2007), they are poorly characterized and understood and hence introduce the large uncertainties in the estimation of climate effect. The largest source of uncertainties in estimating the effect of aerosols on climate is due to the lack of comprehensive database, inadequate information on the temporal and spatial distribution of aerosols and their associated properties, particularly their vertical properties across the globe (Pilinis et al., 1995). Recently, it has been shown that the observations on vertical distribution of aerosols are of paramount importance and a major source of uncertainty in the estimation of atmospheric radiative forcing (Haywood and Ramaswamy, 1998; Chung et al., 2005; Ganguly et al., 2009). The region specific nature of aerosol properties and their consequence on the radiative forcing over the Indian region has been addressed recently by many investigators (e.g. Satheesh et al., 1999; Babu et al., 2002, 2004; Dey and Tripathi, 2008). In most of these studies, the surface properties are attributed to the column by making assumptions about the vertical profiles. However, when the amount of absorbing aerosols (such as soot and mineral dust) is significant, the altitude of aerosol layer as well as its types also becomes important (Satheesh, 2002). Thus, the vertical distribution of aerosols assumes significance. Normally, these vertical profiles are studied by using ground based LIDAR measurements (Devara et al., 1995; Jayaraman et al., 1995; Ramana et al., 2004; Gadhavi and Jayaraman, 2006; Ganguly et al., 2006; Satheesh et al., 2006; Niranjan et al., 2007) or in situ measurements from aircraft (Moorthy et al., 2004; Tripathi et al., 2005a, 2007). LIDAR probing of the atmosphere has gained more popularity in the recent years as they are providing useful information on the vertical profile of aerosols over a wider region such as during the Indian Ocean Experiment (INDOEX) (Ansmann et al., 2000; Müller et al., 2001; Pelon et al., 2002), Southern African Regional Science Initiative

* Corresponding author at: Center for Atmospheric and Oceanic Sciences, Indian Institute of Science, Bangalore 560012, India. Tel.: +91 080 22932505, +91 080 23600450; fax: +91 080 23600 865.
E-mail addresses: dumka@caos.iisc.ernet.in, ucdumka@gmail.com (U.C. Dumka), krishnamorthy_k@vssc.gov.in (K.K. Moorthy), snt@iitk.ac.in (S.N. Tripathi).

1364-6826/$ - see front matter © 2011 Elsevier Ltd. All rights reserved.
doi:10.1016/j.jastp.2011.04.002

campaign (SAFARI-2000) (Eck et al., 2003; McGill et al., 2003) and Aerosol Characterizations Experiment (ACE-II) (Flamant et al., 2000). These LIDAR and aircraft based measurements are quite expensive and technically challenging and also difficult to carry out at hilly terrains of the Himalayas. Therefore, considering the advantage of sharply increasing altitude from ~330 m above mean sea level (amsl) at Haldwani just at the foothills to 1950 m amsl atop of the Manora Peak in the central Himalayan region within a spatial distance of ~10,000 m, we have studied the altitude variation of aerosol properties. The ground based measurements have been made at different altitude levels from the foothills to the peak on the same day. In this paper, we present some interesting features on the altitude profile of spectral aerosol optical depths (AODs), mass concentration (M_b) of aerosol black carbon and total number concentration of composite aerosols near the surface, based on the observations taken from a number of places between continental plains and the mountain peak, during the winter months of 2005, 2006 and 2007. The results and implications of these observations are discussed in the following sections of the manuscript.

2. Observations and data analysis

The experimental measurements were made at a number of places between Haldwani (29.2°N, 79.5°E; ~330 m amsl), a low altitude station at the foothills of the Kumaun ranges of Himalayas (ranges between 28.7° and 30.8°N latitude and 78.7° and 81°E longitude), and Manora Peak, Nainital (29.4°N, 79.5°E; ~1950 m amsl) located at an areal distance of ~10,000 m north of Haldwani, using the different set of instruments carried out in a small motor car. Measurements were also made at locations en route, off from the main road. A map of the study region is shown in Fig. 1. Detailed account of the topographical features of the observational site is presented elsewhere (Dumka et al., 2008).

The measurements were carried out during the winter seasons (November–February) in years 2005, 2006 and 2007. The measurements are available for a limited period due to the large traffic to the hill stations (which is a summer resort). Details of measurements in each year are given in Table 1. The spectral AODs were measured using a hand-held Microtops-II Sun Photometer at central wavelength (λ) 0.38, 0.44, 0.50, 0.675, 0.87 and 1.025 μm using narrow band filters having a full-width at half–maximum of 4 nm at 0.38 μm and 10 nm at longer wavelengths and a field of view ~2.5° (http://www.solar.com; Morys et al., 2001; Porter et al., 2001; Ichoku et al., 2002). The narrow field of view (FOV) of the Microtops-II system (~2.5°) allows only small amount of diffused radiation to enter into the optical assembly. The AODs were derived from the instantaneous solar flux measurements using the instruments internal calibration constants. The Microtops used in this study was factory calibrated prior to the experiment and the measurements were made with extreme care following the considerations given in Morys et al. (2001); Porter et al. (2001) and Ichoku et al. (2002). While making measurements the instrument was carefully held with the sun's image aligned with the cross-wire and five scans were taken in quick succession. If the maximum difference in these five values were more than 0.03, then the lowest three values were accepted and were averaged, because any pointing error would result in a higher AOD. A hand-held Global Positioning

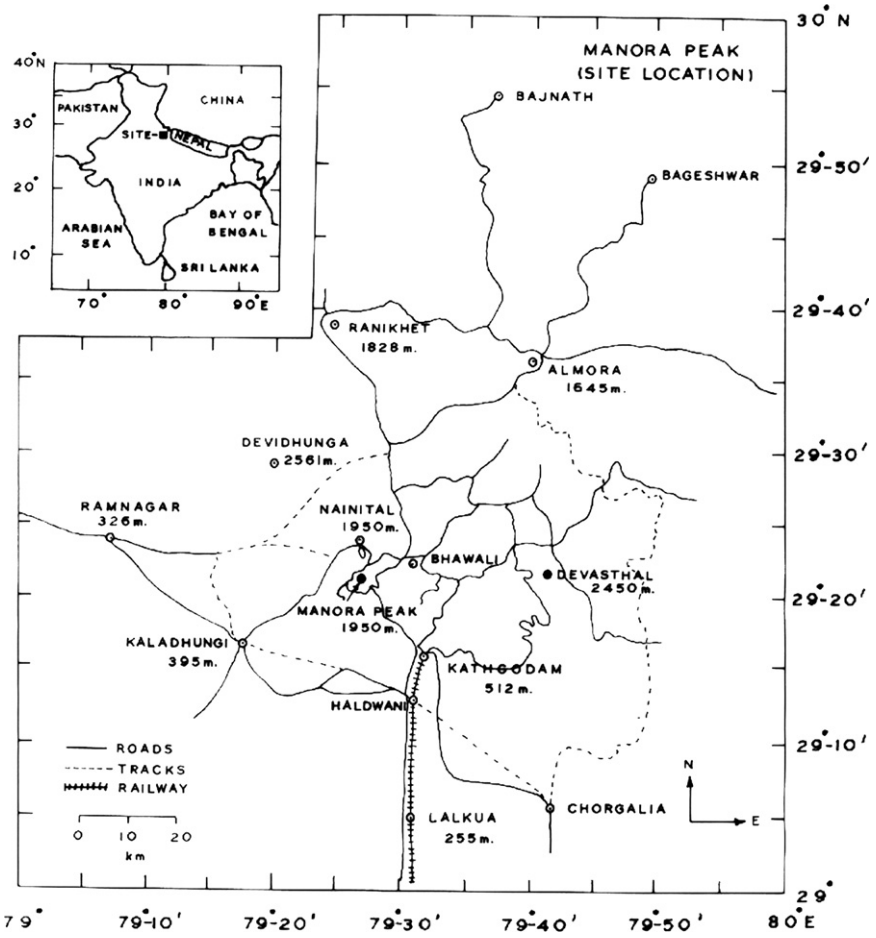

Fig. 1. The road map of the observational site along with the map of India marked with Nainital.

Table 1
Table for *AOD* at 500 nm for three different altitudes and the percentage of contribution of near surface aerosols to columnar *AOD*s at three different levels are presented here.

Date	*AOD* at 500 nm			Percentage contribution of near surface aerosols to columnar *AOD*s %		
	Haldwani	1000 m	Manora Peak	$\Delta\tau_{<1000\ m}$	$\Delta\tau_{<(1000-2000)\ m}$	$\Delta\tau_{>2000\ m}$
7 January 2005	0.292	0.102	0.036	65	23	12
25 February 2005	0.193	0.071	0.038	63	17	20
8 November 2005	0.161	0.133	0.035	17	61	22
22 November 2005	0.648	0.261	0.031	60	35	05
30 November 2005	0.24	0.13	0.047	46	35	20
7 December 2005	0.436	0.232	0.034	47	45	08
28 December 2005	0.33	0.285	0.055	14	70	17
29 December 2005	0.906	0.41	0.042	55	41	05
5 January 2006	0.316	0.124	0.025	61	31	08
12 January 2006	0.583	0.246	0.042	58	35	07
21 January 2006	0.382	0.192	0.055	50	36	14
28 January 2006	0.456	0.358	0.106	21	55	23
3 February 2006	1.063	0.688	0.053	35	60	05
3 January 2007	0.512	0.163	0.055	68	21	11
5 January 2007	0.335	0.15	0.031	55	36	09
16 January 2007	0.926	0.65	0.072	30	62	08
23 January 2007	1.145	0.415	0.068	64	30	06

System (GPS) receiver attached with the Sun Photometer provided the information on the location, time, altitude, pressure and temperature at the place of measurements. The instrument has been in extensive use as part of several campaigns (e.g., Pant et al., 2006) and the protocols were followed precisely. Detailed account on the error budget in the AOD measurement using Sun Photometer is given by Russell et al. (1993) and the error in the AOD measurements is accounted ~5–10% and which is higher for the lower AOD values (Kaskaoutis et al., 2006; Badarinath et al., 2007). A typical uncertainty in such measurements is ± 0.03. On an average, AODs were measured at every 100 m change in altitude, from an en route location of the road.

The other parameters measured are mass concentration (M_B) of black carbon and total number concentration (N_T) of composite aerosols at near surface. The near-real-time M_B was measured using a portable aethalometer (AE-42 of Magee Scientific; USA; http://www.mageesci.com), while the number concentration of composite aerosols near surface was measured using an Optical Particle Counter (OPC; Model no. 1.108 of Grimm Aerosol Technique, GmbH, Germany). The instruments were placed inside the motor car and the sample inlet was mounted ~3 m above the ground level by making a special arrangement. The Aethalometer sampled ambient air through its inlet pipe from an altitude of ~3 m above the ground, at a standard mass flow rate of 5 L min^{-1} with a time base of 2 min. The measured optical attenuation is converted to M_B using an effective absorption coefficient of ~16.6 $m^2\ g^{-1}$ (Hansen, 1996; Babu et al., 2004). Further any negative value of M_B recorded by the aethalometer due to the insufficient time for flow rate adjustment was discarded. The uncertainties in the estimates of M_B are around 10% of the measured values (Hansen, 1996; Babu et al., 2004); however, there are several reports available in the recent years on the uncertainties in the aethalometer measured BC mass concentration (Bodhaine, 1995; Weingartner et al., 2003; Sheridan et al., 2005; Arnott et al., 2005; Corrigan et al., 2006). Weingartner et al. (2003) have suggested two correction factors arising because of the multiple scattering effects in the filter tape (so-called "*C*" factor) and the "shadowing" effects ("*R*" factor). The "*C*" factor arises due to the amplification of the attenuation due to multiple scattering of light that passes through filter tape matrix and the "*R*" factor arises due to "shadowing" by the particles that load the filter tape while sampling, which result in a decrease in the optical path in the filter and thus an underestimation of BC at higher particle loads. While the former tends to overestimate BC, the latter somewhat under estimates it and in a way compensates partly the effect of the former. On the basis of detailed analysis and several experiments, Weingartner et al. (2003) found that the "shadowing" effect and "*R*" factor are quite significant for "pure" soot particles, while almost negligible for aged atmospheric aerosols (which is a mixture). For the mixed aerosols, they estimated the "*C*" factor to be ~2.1. In our measurements, we used an instrument factor 16.6 $m^2\ g^{-1}$ (given by the manufacturer). It accounts for a "*C*" factor (of 1.9 as suggested by the manufacturer) and an "*R*" factor derived from comparison with other techniques, so as to have the effective instrument factor of 16.6 $m^2\ g^{-1}$ at 0.88 μm. In the present study, the "*R*" factor was ignored (considered as unity). This is considered as a "reasonable approximation" in view of the fact that the measurement site was quite far from any strong source. The BC measured at 0.88 μm wavelength is considered to represent a true measure of BC in the atmosphere as at this wavelength BC is the principal absorber of light, while the other aerosol components have negligible absorption (Bodhaine, 1995) and, therefore, BC values at this wavelength are considered here for further analysis as in the case of several earlier works (Ramachandran and Rajesh, 2007; Moorthy et al., 2009; Favez et al., 2009; Cheng et al., 2010). The necessary correction to the measured values of M_B was made to adjust the change in pump speed with change in ambient pressure as the altitude changes, following the considerations given by Moorthy et al. (2004) and further details are given in recent papers (Tripathi et al., 2007; Dumka et al., 2010; Babu et al., 2011). The data analysis involved correcting the Aethalometer measured BC mass concentration for changes in ambient pressure and temperature as the Aethalometer flow was set to operate at a standard mass flow condition (standard temperature $T_0=293$ K and pressure $P_0=1013$ hpa). This was carried out following Moorthy et al. (2004):

$$M_b = M_B\left[\frac{P_0T_1}{P_1T_0}\right]^{-1} \quad (1)$$

where M_B is the raw concentration BC mass; M_b is the true concentrations at standard temperature and pressure (STP), while P_1 and T_1, respectively, are the ambient pressure and temperature. Following the above equation each measurement of BC mass

concentration was converted to true BC mass concentration which is used for further analysis in the present case.

The OPC is a small portable unit, used for the continuous measurements of particles in the ambient air. This instrument enables real-time measurements of ambient aerosol number concentration under varying environmental conditions. The measurements were carried out in number mode, i.e., particle counts as counts per liter with a standard flow rate of 1.2 L min^{-1} with a time base of 1 min. This instrument uses the laser scattering technique for single particle counts, whereby a semiconductor laser serves as the light source, while it is capable of counting from 1 particle L^{-1} to 2 million particles L^{-1}. The scattered signal from the particle passing through the laser beam is collected at approximately 90° by a mirror and transferred to a recipient diode. The pulse height discriminator sets the size range and the number of pulses corresponds to the number of particles. The instrument measures the cumulative number concentration in 15 channels in the range >0.3 to >20 μm with a detection range in 1–10^6 counts L^{-1} with a sensitivity of 1 particle L^{-1}. The counts are used to get the number density i.e. distribution in 15 channels in the range from 0.3 to 20 μm. These numbers are concentrated to mass by assuming spherical particles and a mean particle density of 1.66 g cm^{-3}. Details of the instruments, principle of measurements and analysis are available elsewhere (http://www.grimm-aerosol.com; Pant et al., 2006).

As these two instruments need a stable environment to operate for a smaller period to get the reliable data, they were operated only at convenient locations where they could be taken to a region at least ~50 m off the road and upwind to avoid any possible contamination from local traffic. This ensured that the sampling is not directly affected by any local traffic or source and measurements were done for the air in the ambient atmosphere. As such the altitude resolution is much poorer in the case of BC mass and total number concentration of composite aerosols. The data of aethalometer and OPC averaged for each altitude level are presented here with the corresponding standard deviations.

3. Results and discussions

3.1. Altitude profile of AOD, BC and composite aerosols

The typical altitude variations of AODs at three different wavelengths (0.38, 0.50 and 0.87 μm) are shown in Fig. 2a for 12 January 2006 (solid lines) and 3 January 2007 (dotted lines). The horizontal bars at respective mean values indicate the standard error. In general, the AODs decrease with increase in altitude. It was observed that the AODs at shorter wavelengths appear to respond rapidly to the increasing altitude than the longer wavelengths and above about 1500 m, these tend to merge with each other. This behavior indicates (i) a decrease in abundance of the particles with altitude and (ii) a change in the spectral dependence of the AOD with altitude (i.e., the altitude variation of the Ångström exponent α, which describes the spectral dependence of the AOD). The altitude, above which the AODs show less variability, lies in the range of 1000–1500 m (see Fig. 2a). At the peak (i.e., Manora Peak, Nainital), the AOD values are very low (≤ 0.1 at 0.50 μm), while at the plains (Haldwani) it is as high as 0.5–0.6, which implies that about 80% of the total AOD (at ground level) is due to aerosols within 1000 m. Further, we have also examined the percentage contribution of "near surface" aerosol (where we define the near surface as the lowest point of the profile) to columnar AOD at three different levels (below 1000, between 1000 and 2000 and above 2000 m) and these values are given in Table 1. The AOD (at $\lambda=0.50$ μm) values at Haldwani (lowest altitude of the profile), at 1000 m and at Manora Peak (~2000 m; highest point of the profile) are also listed in Table 1. The percentage contributions of these three regions range between 14% and 68% (with mean value of 48%), 17% and 70% (with mean value of 41%), and 5% and 23% (with mean value of 12%). It can be seen from Table 1 that during the winter period near surface aerosol contribution is high (about 68%) due to the less convective activity, as the surface temperature is low during the period under investigation. This indicates that during the winter season a major fraction of columnar optical depth is contributed by aerosols below 1000 m. Satheesh et al. (2006), from an observational study of vertical distribution of aerosols over an urban continental location, Bangalore, reported that during the winter season the contribution of near surface aerosols to the columnar optical depth ranges between 60% and 80%. The starting and ending time of the different AOD profiles along with the peak altitudes and corresponding time is presented in Table 2. Here, * and ** represent the weak and strong peaks, respectively. A composite plot of the altitude profile of AODs (at 0.50 μm) during the period under study is shown in Fig. 2b. In general, a similar type of altitude variation is obtained except for five days (22 November 2005, 29 December 2005, 3 February 2006, 16 and 23 January 2007), where AOD values below 1200 m were rapidly increasing with decreasing altitude. This is attributed to the dense haze observed during these days. In addition to that, this could be attributed to the evolution of atmospheric boundary layer.

Fig. 3a and b presents the altitude profile of corrected aerosol black carbon and aerosol number density along with the normalized vertical gradient of AOD ($\tau_{ng}=(\delta\tau/\delta h)/\tau$), estimated from values of AOD at different altitudes on the same day as discussed above. The solid points in Fig. 3a and b represent the mean value at each altitude level and the horizontal bars through the points represent the standard error of the mean, a statistical parameter signifying the uncertainty in BC at the respective heights due to the natural atmospheric variabilities.

Following Sasano et al. (1982), we use this parameter to identify the top of the well-mixed region (or the aerosol mixing height), where the normalized gradient peaks sharply. From Fig. 3a and b, it is clearly seen that the mixing height is varying between 1000 and 1500 m which prevailed around 10–12 h local time on the two days. From the altitude profile of BC and number density, it is clearly seen that the BC as well as number concentration shows a sharp decrease up to the top of the mixed layer, above which its altitude variation is very small. The concentration of BC as well as number density is reducing almost by a factor of >2 (for BC) and >15 (for number density) from ground to top of the mixing region. The rapid decrease below the mixing height is attributed due to the well-mixed nature of aerosols, so that their concentration decreases in line with that of the other atmospheric species. A composite plot of the altitude variation of BC, number density along with the normalized vertical gradient of AOD at 0.44 and 0.50 μm during all the observational days is presented in Fig. 3c.

The spectral variation of AODs provides the useful information regarding the columnar size distribution and it can be best represented by Ångström power law of the form $\tau_{p\lambda}=\beta\lambda^{-\alpha}$, where α is the Ångström wavelength exponent, β (equal to τ_p; at $\lambda=1$ μm) is the Ångström turbidity parameter and λ is the wavelength in μm (Ångström, 1961). The Ångström wavelength exponent α depends on the size distribution of aerosols and is a measure of the ratio of the concentration of coarse to accumulation mode aerosols, with higher values representing increased abundance of accumulation mode aerosols, whereas β depends on the total aerosol loading in the atmosphere (Satheesh and Moorthy, 1997; Dumka et al., 2008). The Ångström parameters (α and β) for each day are obtained by performing a linear

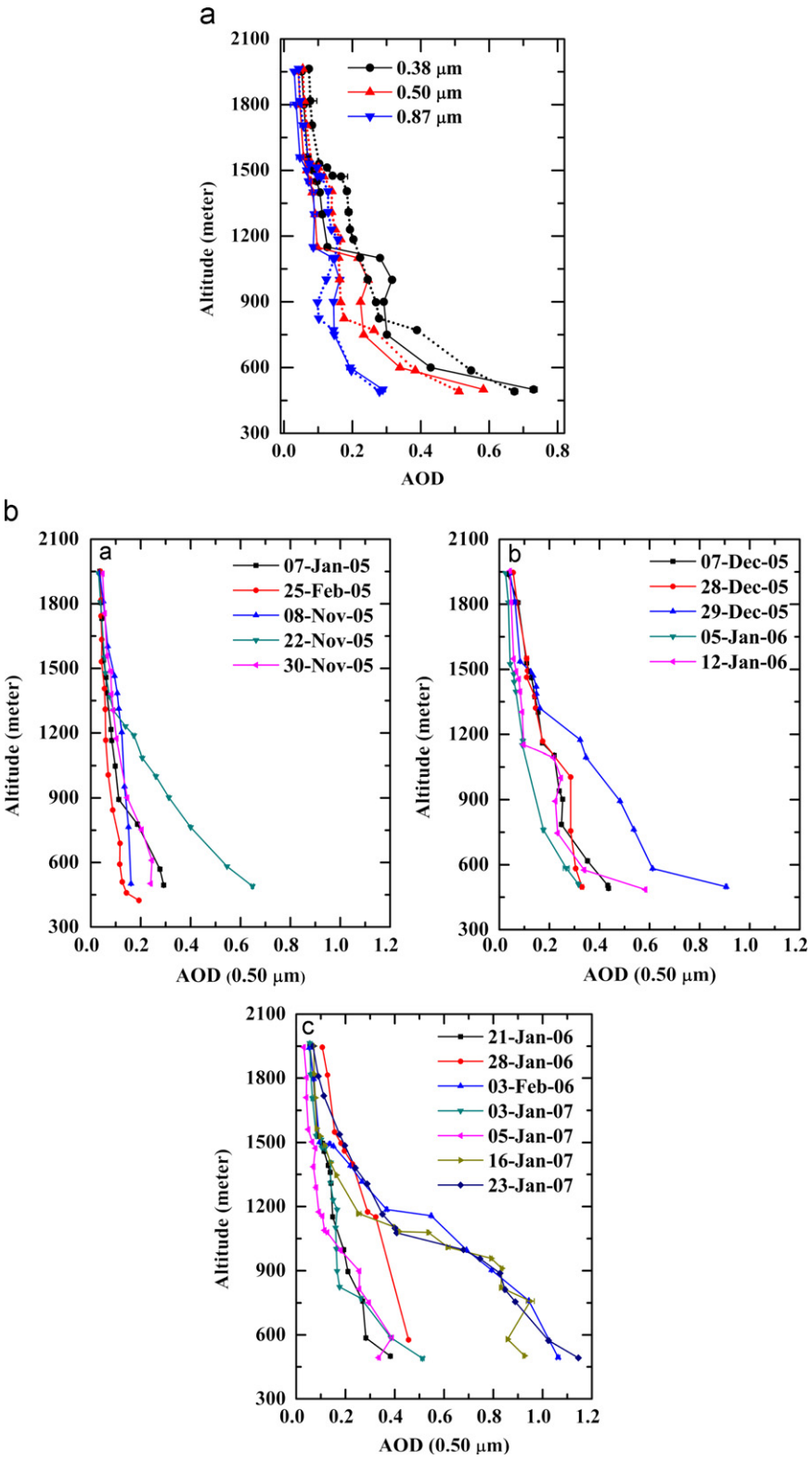

Fig. 2. (a) Altitude profiles of AOD at three different wavelengths 0.38, 0.50 and 0.87 μm for 12 January 2006 (solid lines) and 3 January 2007 (dotted lines). The each solid point represents the AOD value irrespective of the altitude and the horizontal bars through each solid point represent the standard error. (b) Composite altitude profiles of AOD at 0.50 μm for all the observational days.

regression analysis on the individual AOD spectra on log–log scale. The typical altitude variations of α and β on the same days as discussed above are shown in Fig. 4a. The horizontal bars at the respective values of α and β indicate the errors in the estimation of α and β. Also a composite plot of the altitude variation of α and β during all the days of observation is shown in Fig. 4b. From Fig. 4a and b, it can be clearly seen that the both α and β values are very high at Haldwani (lowest point of our profile), which

Table 2
Table for the starting and ending time of the different *AOD* profiles along with the peak altitude and corresponding time. Here, * and ** represent the weak and strong peaks, respectively.

Date	Time (HH:MM:SS)		Peaks in altitude profile of AOD					
	Start	End	Altitude (m)			Time (HH:MM:SS)		
			1st	2nd	3rd	1st	2nd	3rd
7 January 2005	7:57:03	13:08:19	900**	–	1500*	11:50:46	–	9:30:43
25 February 2005	8:51:16	13:24:13	–	–	1500*	–	–	10:34:45
8 November 2005	6:53:50	14:03:20	–	–	–	–	–	–
22 November 2005	7:23:03	13:32:01	–	1250**	–	–	10:35:05	–
30 November 2005	8:06:44	14:46:47	850**	–	1500**	12:38:04	–	10:04:36
7 December 2005	7:16:45	14:21:42	700	1100	1500*	13:09:44	12:38:36	9:26:10
28 December 2005	7:44:25	15:30:11	–	1100	1500*	–	13:26:45	10:24:41
29 December 2005	7:29:18	15:14:55	–	1200*	1500*	–	13:02:08	10:03:03
5 January 2006	7:36:49	15:28:08	–	–	1500	–	–	9:56:54
12 January 2006	8:05:30	15:48:28	–	1100	1500*	–	11:23:50	9:55:17
21 January 2006	7:41:25	14:55:43	900*	1100*	1500**	12:55:53	12:34:45	9:31:29
28 January 2006	7:52:15	12:11:35	–	1150**	1500*	–	11:17:42	9:44:27
3 February 2006	7:52:37	13:06:30	–	1200	1500**	–	11:20:51	9:31:39
3 January 2007	7:55:47	14:04:00	800*	–	1500**	12:32:38	–	9:47:15
5 January 2007	7:35:34	13:48:26	750*	1000**	1500	12:14:03	11:25:16	9:20:20
16 January 2007	7:53:39	13:55:19		1000**	–	–	11:15:05	–
23 January 2007	7:50:00	13:54:39	–	1100	–	–	11:44:34	–

signifies the high aerosol loading, with a dominance of submicron size aerosol particles. As the altitude increases, initially the β decreases rapidly, implying a large reduction in the aerosol loading. However, α remains nearly steady up to ~1000–1500 m, suggesting that the reduction occurs in the abundance of accumulation and coarse mode particles almost equally, so that the size spectrum is not much affected. This is mainly attributed to the strong thermal convections in the plains, which thoroughly mix the particles of different sizes. Between 1000 and 1500 m α remains low, suggesting a flat size spectrum. This approximately would be coinciding with the top of the boundary layer, where the inversion shields the convective eddies from propagating higher. This is supported by the almost altitude invariant nature of β. However, above 1500 m, α again increases with increasing altitude, and β decreases to very low values, suggesting highly reduced abundance in the "free troposphere"; the concentration above being maintained by the smaller particles that have longer residence time and are also amenable to long-range transport.

3.2. Aerosol size distribution

As the spectral characteristics of aerosol optical depth have an imprint of the aerosol (columnar) size distributions (CSDs), it is possible to estimate the size distribution of aerosols form the spectral aerosol optical depth measurements. Out of several available methods for inverting the aerosol columnar size distributions, the constrained linear inversion technique (King et al., 1978; King, 1982) has been used in the present case. This inversion technique involves the numerical inversion of the Mie integral equation given by

$$\tau_p(\lambda) = \int_{r_a}^{r_b} \pi r^2 Q_{ext}(r,m,\lambda) n_c(r) dr \quad (2)$$

where Q_{ext} is the aerosol Mie extinction efficiency parameter, which is a function of the aerosol complex refractive index (m), radius (r) and wavelength of the incident radiation (λ); $n_c(r)$ is the columnar number density of aerosols (in a vertical column of unit cross section) in an infinitesimal radius range dr centered at r. In defining the $n_c(r)$ this way, it is implicitly assumed that the number size distribution is height invariant or averaged over the vertical column. The radii limits r_a and r_b to the integral are, respectively, the lower and upper cut-off radii of the particles, such that only those particles having sizes within the range r_a–r_b contribute significantly to Q_{ext}. Both r_a and r_b depend strongly on the shortest and longest wavelengths of the AOD spectra (King, 1982) and are taken as 0.05 and 3.0 mm, respectively, in line with Moorthy et al. (1997). The aerosols are assumed as spherical. The technique involves discretizing the above integral via quadrature formulae and solving the resulting matrix equation for $n_c(r)$ following the iterative inversion procedure described in King (1982). More details of the application of this technique to the spectral AOD data have been discussed in the literature (e.g. Moorthy et al., 1997; Saha and Moorthy, 2004; Gogoi et al., 2009; Dumka et al., 2009). A composite plot for all the columnar size distributions is shown in Fig. 5a and b. Each day's figure has two panels, the lower panel of each figure represents the retrieved columnar size distributions in a log–log scale at three different altitudes, while the upper panel (a) the measured AODs (by solid points with error bars) and the AODs re-estimated from the columnar size distributions (by continuous line) are plotted as a function of wavelength. The retrieved CSD, obtained from spectral AOD measurements, shows a power law, unimodal as well as bimodal (a combination of power law and unimodal log normal distribution) size distribution with a prominent secondary peak (coarse mode) occurring at large value of radius (>0.5 μm), while the primary (fine mode) does not appear explicitly. From the CSDs, the following physical parameters were estimated as a function of altitudes: (i) total columnar content (N_T), (ii) number concentration of the accumulation and coarse mode (N_a and N_c), (iii) columnar mass loading (M_L) and (iv) effective radii (R_{eff}). The detailed information regarding these physical parameters at three different altitudes (Manora Peak, 1000 m and Haldwani) are given in Table 3.

In addition to the above, the number size distributions of boundary/surface layer aerosols are estimated from the individual measurements of OPC data. All these size distributions consistently revealed a bimodal size distribution over the entire altitude range with a secondary coarse mode particle at ~1 μm, while the primary mode does not appear because of the large lower cut-off of the OPC. A composite size distribution of near surface aerosols is also shown in the same Fig. 5a and b by dotted line and the physical parameter of these size distributions at three different altitudes is listed in Table 4.

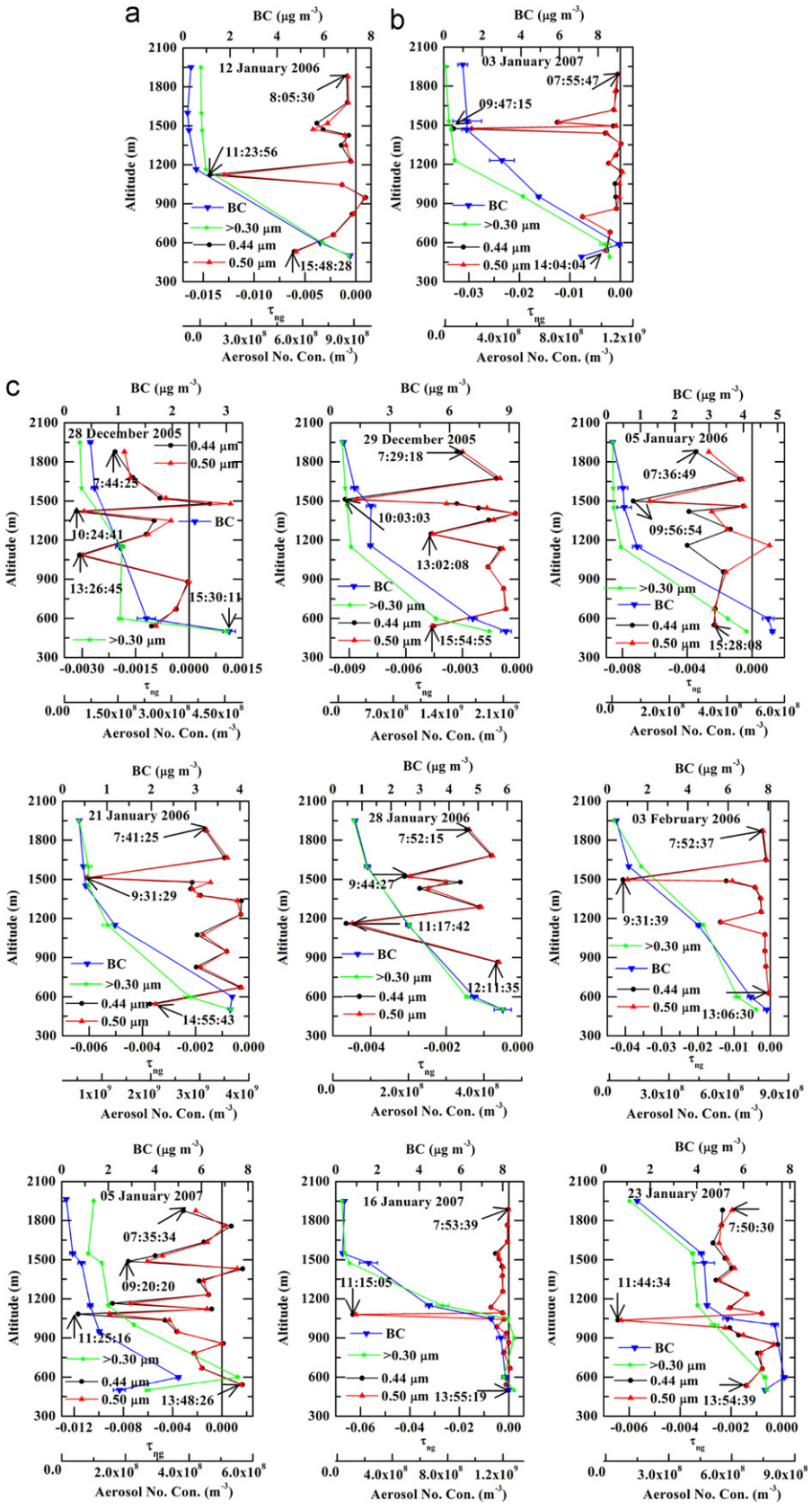

Fig. 3. (a) Altitude profiles of M_b and N_T along with the normalized vertical gradient of AOD at 0.44 and 0.50 μm for 12 January 2006. The arrow mark in the gradient plot shows the starting, ending and peaking time of the profiles. (b) Altitude profiles of M_b and N_T along with the normalized vertical gradient of AOD at 0.44 and 0.50 μm for 3 January 2007. The arrow mark in the gradient plot shows the starting, ending and peaking time of the profiles. (c) A composite plot of altitude variation of M_b and N_T along with the normalized vertical gradient of AOD at 0.44 and 0.50 μm for all the observational days.

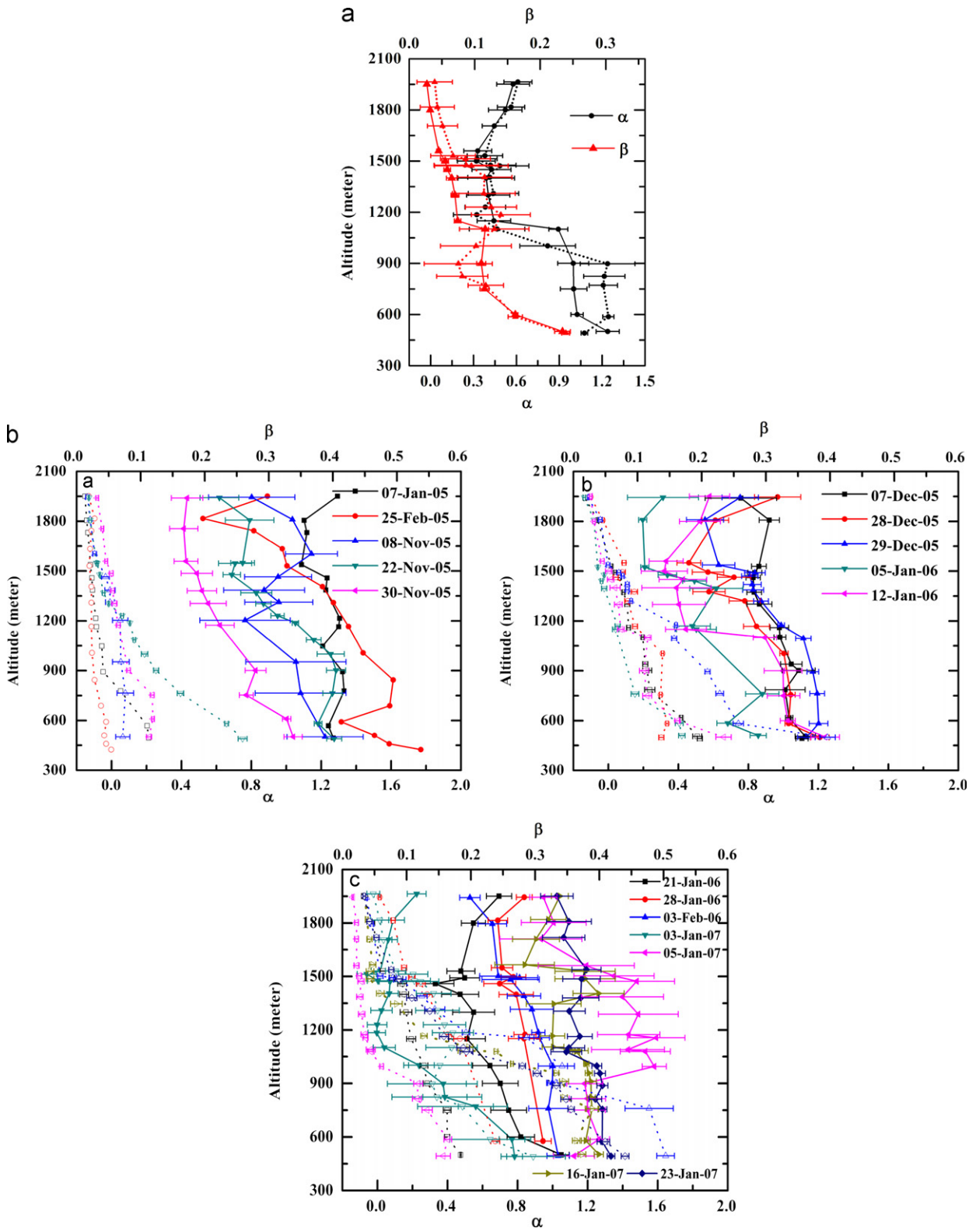

Fig. 4. (a) Altitude profiles of Ångström parameters (α and β) for 12 January 2006 (solid lines) and 3 January 2007 (dotted lines). The horizontal bars through each solid point represent the error in the estimation of the Ångström parameters irrespective of the altitude. (b) A composite plot of Ångström parameters (α and β).

A comparison between CSDs and the boundary layer aerosol size distributions (or number size distribution near surface) is found to be in good agreement, especially in its nature of variation with size. The estimated parameters differed, primarily because those retrieved from the AOD data pertained to the column, while those from the OPC pertained to the ambient. As such, N_T would be much higher in the column. However, parameters such as effective radius were more or less comparable. We found that the share of sub-micron and super-micron aerosol to the total aerosol concentration (for both in column and surface) indicates the dominant role of sub-micron aerosols and it accounts for $>90\%$ of total particles.

3.3. Vertical distribution of heating rate due to BC absorption

In order to estimate the aerosol radiative effects from the microphysical measurements, an appropriate aerosol model is required which has the information like aerosol chemical composition, size distributions as well as altitude distributions. In general, a hybrid approach is followed using the observations to constrain the aerosol model (Babu et al., 2002; Satheesh et al., 2002; Vinoj and Satheesh, 2003; Moorthy et al., 2005; Satheesh and Srinivasan, 2006; Ramachandran and Kedia, 2010). This hybrid approach involves two steps: (i) the derivations of aerosol optical properties (such as aerosol optical depth, single scattering

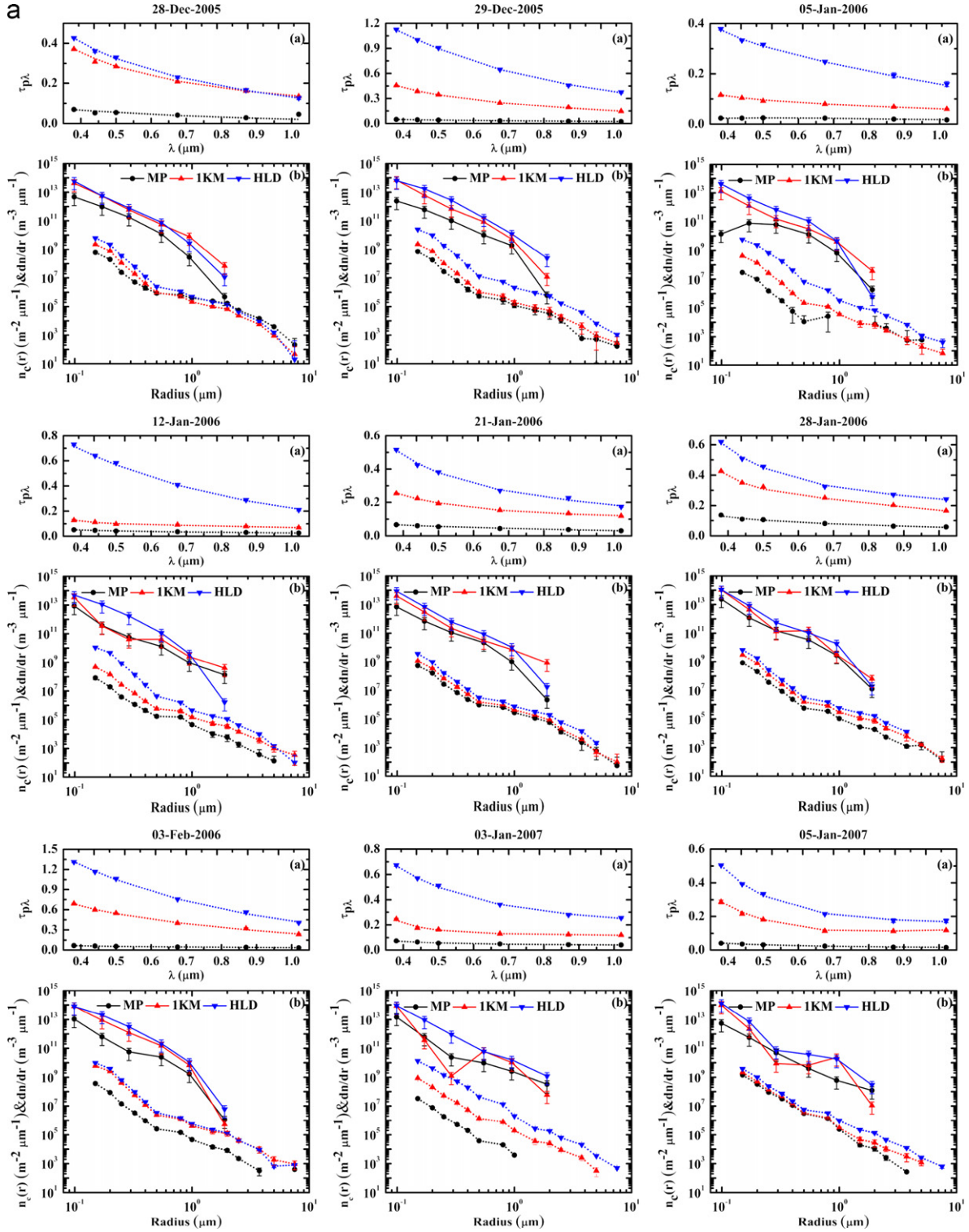

Fig. 5. (a, b) Composite plot of aerosol number size distribution for columnar as well as near surface aerosols during study period at Manora Peak, ~100 m and Haldwani, respectively. Bottom panel (b) shows CSD obtained from the inversion of spectral AOD (continuous line joining the points) along with the number size distributions at the surface obtained from the OPC data (dotted line) and top-panel shows the AOD values obtained from Microtops-II (points with error bars) and those re-estimated from the CSD shown below (by dotted line).

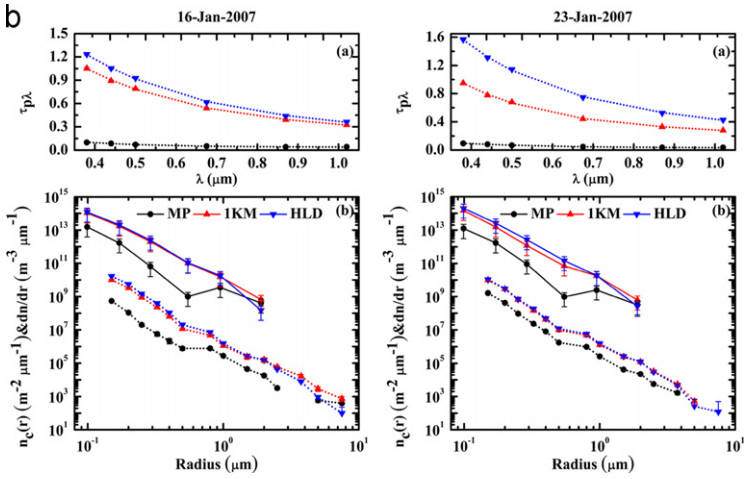

Fig. 5. (*continued*)

Table 3
Table for total number concentration (N_T), coarse mode concentration (N_c), mass loading (M_L) and effective radius (R_{eff}) for columnar aerosols at three different altitudes as given in Table 1.

Date	Total number concentration (N_T), coarse mode concentration (N_c), mass loading (M_L) and effective radius (R_{eff})											
	Manora Peak				~1000 m				Haldwani			
	N_T	N_c	M_L	R_{eff}	N_T	N_c	M_L	R_{eff}	N_T	N_c	M_L	R_{eff}
28 December 2005	4.4E+11	1.85E+09	17.82	0.24	3.84E+12	1.34E+10	121.82	0.25	5.57E+12	1.24E+10	121.59	0.20
29 December 2005	2.40E+11	2.60E+09	17.58	0.34	6.44E+12	1.57E+10	140.40	0.20	5.69E+12	3.18E+10	307.50	0.27
5 January 2006	2.19E+10	2.29E+09	10.20	0.49	1.25E+12	7.15E+09	47.34	0.29	3.89E+12	1.81E+10	120.82	0.24
12 January 2006	8.73E+11	2.67E+09	18.92	0.22	3.72E+12	7.88E+09	52.57	0.18	4.53E+12	1.88E+10	185.81	0.24
21 January 2006	6.49E+11	3.75E+09	23.03	0.26	3.72E+12	1.03E+10	95.73	0.25	7.90E+12	1.93E+10	170.08	0.21
28 January 2006	2.29E+12	6.88E+09	48.72	0.22	9.94E+12	2.40E+10	154.74	0.18	1.00E+13	2.68E+10	226.63	0.22
3 February 2006	1.02E+12	4.59E+09	25.95	0.24	7.54E+12	2.57E+10	205.50	0.22	7.44E+12	3.76E+10	349.79	0.25
3 January 2007	1.45E+12	3.57E+09	30.80	0.23	1.06E+13	1.65E+10	123.74	0.17	8.25E+12	2.05E+10	243.31	0.26
5 January 2007	4.98E+11	1.14E+09	10.14	0.18	8.83E+12	1.16E+10	138.10	0.20	1.19E+13	1.66E+10	198.69	0.19
16 January 2007	1.37E+12	2.52E+09	41.22	0.27	9.73E+12	2.59E+10	313.76	0.24	1.10E+13	2.85E+10	352.20	0.23
23 January 2007	1.09E+12	1.92E+09	31.79	0.24	1.33E+13	2.26E+10	285.06	0.20	1.86E+13	3.46E+10	432.47	0.20

Table 4
Table for total number concentration (N_T), coarse mode concentration (N_c), mass loading and effective radius for near surface aerosols at three different altitudes as given in Table 1.

Date	Total number concentration (N_T), coarse mode concentration (N_c), mass loading (M_L) and effective radius (R_{eff})											
	Manora Peak				~1000 m				Haldwani			
	N_T	N_c	M_L	R_{eff}	N_T	N_c	M_L	R_{eff}	N_T	N_c	M_L	R_{eff}
28 December 2005	1.79E+07	5.64E+04	4.63E−04	2.63E−01	6.81E+07	2.21E+04	6.93E−04	1.30E−01	1.93E+08	4.66E+04	1.94E−03	1.26E−01
29 December 2005	1.92E+07	1.10E+04	2.48E−04	1.63E−01	6.71E+07	1.89E+04	7.19E−04	1.38E−01	8.41E+08	1.90E+05	9.43E−03	1.32E−01
5 January 2006	9.01E+05	2.18E+03	1.44E−04	1.16E+00	1.30E+07	2.27E+03	1.51E−04	1.40E−01	2.15E+08	2.39E+04	3.11E−03	1.44E−01
12 January 2006	2.24E+06	2.15E+03	3.73E−05	1.79E−01	1.41E+07	1.31E+04	2.84E−04	2.21E−01	3.87E+08	3.88E+04	3.95E−03	1.22E−01
21 January 2006	1.57E+07	2.08E+04	2.64E−04	1.84E−01	3.36E+07	3.06E+04	5.11E−04	1.67E−01	9.97E+07	6.55E+04	1.21E−03	1.48E−01
28 January 2006	2.23E+07	7.48E+03	2.79E−04	1.57E−01	8.07E+07	2.59E+04	8.46E−04	1.37E−01	3.48E+08	3.41E+05	1.98E−02	2.29E−01
3 February 2006	1.31E+07	8.17E+03	3.84E−04	2.02E−01	2.07E+08	4.08E+04	2.25E−03	1.34E−01	3.22E+08	4.58E+04	3.26E−03	1.26E−01
3 January 2007	2.02E+06	2.94E+05	2.58E−03	7.10E−01	3.25E+07	3.10E+04	1.04E−03	1.96E−01	4.61E+08	6.18E+04	8.06E−03	1.59E−01
05 January 2007	7.54E+07	1.73E+05	4.39E−03	2.18E−01	7.94E+07	4.44E+04	2.43E−03	1.93E−01	1.11E+08	4.82E+04	1.68E−03	1.65E−01
16 January 2007	1.85E+07	3.60E+04	6.14E−04	2.16E−01	3.31E+08	5.62E+04	4.51E−03	1.45E−01	5.54E+08	5.25E+04	7.12E−03	1.37E−01
23 January 2007	8.61E+07	1.45E+05	4.96E−03	2.22E−01	4.02E+08	1.82E+05	1.05E−02	1.67E−01	3.19E+08	4.59E+04	3.78E−03	1.36E−01

albedo and phase function and asymmetry parameter) by using the available observations (AOD spectra and BC mass concentration in the present case) and (ii) incorporation of the derived aerosol optical properties into a radiative transfer model. This method is widely used and well documented in the literature (e.g. Satheesh et al., 1999; Podgorny et al., 2000; Babu et al., 2002; Satheesh, 2002; Conant et al., 2003; Vinoj and Satheesh, 2003; Pant et al., 2006; Moorthy et al., 2009) and estimate the aerosol radiative forcing within the accuracy of ± 2 W m^{-2} (Satheesh and Srinivasan, 2006). In this approach, the Optical Properties of Aerosols and Clouds (OPAC; Hess et al., 1998) database have been used to construct the spectral variation of AODs, SSA, phase function and asymmetry parameter, which are the fundamental parameter for aerosol radiative forcing estimation. In the present paper, we have used

the measured aerosol black carbon mass concentration as an anchoring point and various aerosol species were iteratively varied until agreement (within 5%) was reached between modeled and measured spectral aerosol optical depth. Based on the observed AOD spectra and BC values, the main components of OPAC are considered as water-soluble, insoluble and soot. The aerosol model thus obtained is capable of reproducing the measured spectral aerosol optical depth and has the same amount of aerosol black carbon as measured. The relative humidity is set to 50% and the aerosol properties are calculated for 25 wavelengths in the shortwave region (0.25–4.0 μm). Aerosol spectral optical depths as well as spectral values of single scattering albedo, phase function and asymmetry parameter are used as inputs in Santa Barbara DISORT Atmospheric Radiative Transfer (SBDART) model (Ricchiazzi et al., 1998) to simulate surface reaching solar irradiance for different solar zenith angles. The simulated irradiances are then used to calculate the diurnally averaged aerosol radiative forcing. The detailed methodology followed is available in the literature (Babu et al., 2002; Satheesh, 2002; Satheesh and Srinivasan, 2002; Vinoj and Satheesh, 2003; Vinoj et al., 2004). The Santa Barbara Discrete Ordinate (DISORT) Atmospheric Radiative Transfer (SBDART) model (Ricchiazzi et al., 1998) developed at the University of California, Santa Barbara, USA, which is based on a collection of well-tested and reliable physical models, which were developed by the atmospheric science community over the past few decades, has been used for the radiative transfer calculations. These models are used to estimate aerosol radiative forcing by incorporating the observations and have been used extensively to estimate the aerosol radiative forcing over wide range of environments including the marine, urban, rural and high altitude sites (e.g. Satheesh et al., 2002; Kim et al., 2004; Tripathi et al., 2005b; Lesins et al., 2009; Pathak et al., 2010; Vinoj et al., 2010; Li et al., 2010; Ma et al., 2010). The model atmosphere is assumed to be tropical and the spectral albedo of the surface is assumed as a mixture of vegetation (80%) and sand (20%) following Pant et al. (2006). Radiative transfer calculations are performed with eight radiative streams and the fluxes with and without aerosols are computed every hour. Direct ARF values at the surface and the Top of the Atmosphere (TOA) are then estimated as the difference of the fluxes calculated with and without aerosols. The uncertainties in SBDART calculations arise mainly due to the assumptions of the model atmosphere, optical and radiative properties of trace gases and aerosols and surface albedo, etc. as described in earlier papers (McComiskey et al., 2008; Moorthy et al., 2009). The overall uncertainty in SBDART estimations for this configuration at Nainital is reported to be 15–20% (Pant et al., 2006).

The computed SSA (0.50 μm) varies between 0.44 and 0.83 (with a mean value 0.64 ± 0.04) at higher height and a small increase in SSA (from 0.52 to 0.89; with mean value 0.77 ± 0.03) was found at the surface indicating the significant amount of absorbing aerosols. The SSA values range from 0.45 to 0.90 (with mean value 0.77 ± 0.04) at 1000 m. This SSA value is comparable with Babu et al. (2002) for Bangalore (0.78) and Tripathi et al. (2005b) for Kanpur (0.76). Based on sun–sky radiometer measurements over an urban site (Pune), Pandithurai et al. (2004) have estimated the SSA to be 0.81 for the winter season 2001–2002. The low value of SSA during the period under study is due to the presence of large amount of BC mass concentration. This value of SSA was found to be in good agreement with the values observed by Chinnam et al. (2006). Ramana et al. (2004) have observed the SSA values (0.50 μm) in the range of 0.70–0.90 in the Himalayan region (Kathmandu, Nepal) by combining the actual measurements of scattering and absorption coefficient using a TSI nephelometer and a Particle Soot Absorption Photometer (PSAP). On the other hand, Pant et al. (2006) have estimated the SSA value at Nainital in the range of 0.87–0.94 with the mean value of 0.90 during the month of December 2004. The SSA value reported by Pant et al. (2006) was calculated using the long-term measurements of spectral AOD, while in the present study, we have included the instantaneous measurements of AOD. Also the AOD value at higher altitude is very low (<0.1) and the uncertainty in the AOD measurements using the Microtops-II Sun Photometer is ± 0.03 and therefore, the uncertainty in the retrieved SSA was ~10–15% (Moorthy et al., 2009). The value of SSA and g at 0.50 μm for three respective altitudes are listed in Table 5.

The Aerosol Optical Properties (AOD, α, g and ω) thus deduced from measured altitude profiles are then incorporated in a Discrete Ordinate Radiative Transfer model developed by University of Santa Barbara (SBDART) (Ricchiazzi et al., 1998) along with the other necessary parameters include the solar geometry, a model atmosphere and the surface albedo, to estimate the net radiative fluxes (downward minus upward) at the top and bottom of each atmospheric layer. The aerosol induced flux change at each atmospheric layer is derived from the net radiative flux estimations with and without aerosols. The net flux change due to aerosols between top and bottom boundary of each layer is the flux absorbed in the layer. This radiative flux or energy is transformed into heat and hence the resultant atmospheric forcing values are further used to calculate the lower atmospheric heating rate (Liou, 1980) as follows:

$$\frac{\partial T}{\partial t} = \frac{g}{C_p}\frac{\Delta F}{\Delta P} \tag{3}$$

where $\partial T/\partial t$ represents the heating rate in K day^{-1}, g represents the acceleration due to gravity (9.91 m s^{-2}), C_p is the specific heat

Table 5
Table for absorption Ångström exponent (AAE), single scattering albedo (SSA) and asymmetry parameter (g) at three different altitudes as given in Table 1.

Date	Ångström exponent (AAE), single scattering albedo (SSA) and asymmetry parameter (g)								
	Manora Peak			~1000 m			Haldwani		
	AAE ± SE	SSA	g	AAE ± SE	SSA	g	AAE ± SE	SSA	g
28 December 2005	1.31 ± 0.02	0.64	0.69	1.09 ± 0.02	0.75	0.68	1.04 ± 0.02	0.52	0.61
29 December 2005	1.44 ± 0.04	0.44	0.67	0.88 ± 0.05	0.85	0.68	0.92 ± 0.04	0.79	0.68
5 January 2006	1.83 ± 0.04	0.58	0.74	1.28 ± 0.03	0.71	0.72	1.00 ± 0.02	0.63	0.68
12 January 2006	0.68 ± 0.02	0.63	0.75	0.99 ± 0.12	0.90	0.70	1.24 ± 0.08	0.76	0.67
21 January 2006	1.40 ± 0.03	0.72	0.72	1.00 ± 0.03	0.76	0.70	0.91 ± 0.03	0.80	0.67
28 January 2006	1.12 ± 0.03	0.80	0.70	1.02 ± 0.03	0.81	0.69	0.92 ± 0.03	0.78	0.68
3 February 2006	1.43 ± 0.03	0.66	0.74	1.09 ± 0.04	0.80	0.70	0.89 ± 0.04	0.83	0.68
3 January 2007	1.46 ± 0.03	0.52	0.71	1.06 ± 0.02	0.45	0.61	1.00 ± 0.01	0.74	0.67
5 January 2007	1.05 ± 0.02	0.71	0.66	0.90 ± 0.03	0.84	0.67	0.84 ± 0.03	0.85	0.68
16 January 2007	0.86 ± 0.01	0.83	0.69	1.02 ± 0.02	0.75	0.66	0.90 ± 0.04	0.83	0.67
23 January 2007	1.08 ± 0.02	0.55	0.61	0.94 ± 0.03	0.82	0.66	0.82 ± 0.04	0.89	0.67

Table 6
Table for BC mass concentration (μg m^{-3}), aerosol radiative forcing (W m^{-2}) at surface, top of the atmosphere and atmospheric forcing and heating rate (K day^{-1}) at three different altitudes as given in Table 1. The radiative forcing efficiency at surface, top of the atmosphere and in the atmosphere is also given in the second line against each day.

	BC mass concentration (μg m^{-3}), radiative forcing (W m^{-2}) and heating rate (K day^{-1})														
	Manora Peak					~1000 m					Haldwani				
	BC	SUR	TOA	ATM	HR	BC	SUR	TOA	ATM	HR	BC	SUR	TOA	ATM	HR
28 December 2005	0.48	−5.79	0.77	6.56	0.18	1.02	−13.91	0.57	14.48	0.41	3.05	−32.98	9.15	42.13	1.18
	–	–	–	–	–	–	−48.82	2.01	50.82	–	–	−99.94	27.72	127.66	–
29 December 2005	0.66	−5.75	1.48	7.23	0.20	2.01	−19.06	−2.36	16.70	0.47	8.84	−48.15	1.85	50.00	1.41
	–	–	–	–	–	–	−46.49	−5.75	40.74	–	–	−53.14	2.05	55.19	–
5 January 2006	0.19	−3.37	0.50	3.87	0.11	0.90	−8.43	0.58	9.01	0.25	4.85	−28.45	5.44	33.89	0.95
	–	–	–	–	–	–	−67.97	4.67	72.64	–	–	−90.03	17.23	107.26	–
12 January 2006	0.34	−4.55	0.55	5.10	0.14	0.56	−12.95	−3.55	9.40	0.26	7.11	−36.84	3.46	40.30	1.13
	–	–	–	–	–	–	−52.65	−14.44	38.22	–	–	−63.19	5.94	69.13	–
21 January 2006	0.38	−4.96	0.21	5.17	0.15	1.18	−12.46	0.51	12.97	0.36	3.78	−25.23	0.34	25.58	0.72
	–	–	–	–	–	–	−64.92	2.64	67.56	–	–	−66.05	0.90	66.95	–
28 January 2006	0.76	−8.40	−0.23	8.17	0.23	2.59	−21.99	−0.42	21.57	0.61	4.86	−32.30	2.06	34.36	0.97
	–	–	–	–	–	–	−61.43	−1.17	60.26	–	–	−70.83	4.53	75.36	–
3 February 2006	0.45	−5.69	0.74	6.43	0.18	4.53	−35.29	0.74	36.04	1.01	7.93	−54.77	0.70	55.47	1.56
	–	–	–	–	–	–	−51.30	1.08	52.38	–	–	−51.53	0.66	52.18	–
3 January 2007	0.99	−7.55	1.59	9.14	0.26	4.92	−22.58	6.69	29.27	0.82	7.14	−35.64	3.68	39.31	1.11
	–	–	–	–	–	–	−138.54	41.06	179.60	–	–	−69.60	7.18	76.78	–
5 January 2007	0.19	−2.96	0.25	3.20	0.09	1.61	−12.27	−1.31	10.96	0.31	2.48	−19.48	−2.05	17.44	0.49
	–	–	–	–	–	–	−81.80	−8.72	73.08	–	–	−58.16	−6.11	52.05	–
16 January 2007	0.41	−5.13	−0.46	4.66	0.13	7.45	−36.16	3.39	39.54	1.11	8.28	−43.88	0.28	44.15	1.24
	–	–	–	–	–	–	−55.63	5.21	60.84	–	–	−47.38	0.30	47.68	–
23 January 2007	1.44	−8.82	2.23	11.04	0.31	5.31	−39.54	0.31	39.85	1.12	6.92	−46.79	−3.28	43.50	1.22
	–	–	–	–	–	–	−95.27	0.75	96.02	–	–	−40.86	−2.87	37.99	–

capacity of air at the constant pressure (~1006 J kg^{-1} K^{-1}), ΔF is the atmospheric radiative forcing and ΔP is the atmospheric pressure difference between top and bottom boundary of each layer (Satheesh and Ramanathan, 2000). The value of aerosol radiative forcing, forcing efficiency (defined as the forcing per unit optical depth) at surface, atmospheric and top of the atmospheric and corresponding heating rate along with BC mass concentration (μg m^{-3}) at three altitude levels (below 1000, between 1000 and 2000 and above 2000 m) of measurements is presented in Table 6. Forcing efficiency at Manora Peak (highest point of observations) is not considered in Table 6, because the AOD values at Manora Peak are very low (<0.1), and even a small value of radiative forcing will result into a sufficiently large value of forcing efficiency (because of the very small denominator), which is physically unrealistic because the forcing efficiency under such conditions is only virtual. Therefore, we estimated the forcing efficiency only when the AOD values were >0.1. As such, in Table 6, we have compared the forcing efficiency only for Haldwani and at 1000 m altitude. It is evident that the forcing efficiency changes with altitude indicating that the aerosols present at each altitude are quite different (see Table 6). This comparison shows that the forcing efficiency decreases as we go uphills, showing that the aerosol type is different at higher altitudes from the more polluted one at the lower altitude (Haldwani).

The vertical profiles of atmospheric heating rate due to aerosol absorption thus calculated are shown in Fig. 6. A sharp decrease as a function of altitude up to 1500 m and above that heating rate slowly decreases with altitude except on 28 December 2005 and 23 January 2007, where heating rate is slightly constant from ~1000 to 1500 m and then decreasing with altitudes. A very steep fall in heating rate from surface to 1500 m is also obtained on 3 February 2006. The heating rate varies between 0.09 and 0.31, 0.25 and 1.12 and 0.49 and 1.56 K day^{-1} at Manora Peak, ~1000 m and Haldwani, respectively (see Table 6). Highest radiative heating rate is observed on 3 February 2006 and 23 January 2007 at surface and Manora Peak, respectively. On 16 and 23 January 2007 atmospheric heating rate is almost steady up to ~1000 m, which is

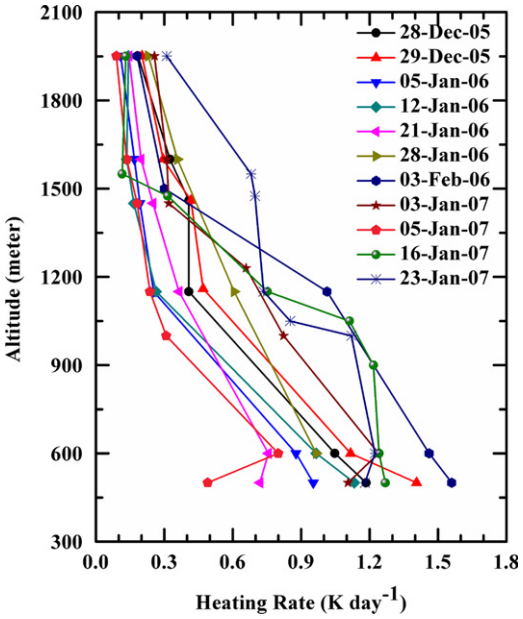

Fig. 6. Altitude profiles of heating rate during the study period.

related to well-mixed aerosols within boundary layer. These variations of radiative heating rate are closely related to the optical properties of aerosols and their vertical distributions. At the surface level, we get the maximum heating rate which is mainly caused by the dominant role of absorbing aerosols produced by the fossil fuel combustion or biomass burning activities nearby the observational site. The higher amount of heating of lower atmosphere can in-turn amplify the formation of winter time inversion layer and thereby impact on the dispersal of aerosols (Ramana et al., 2004). Higher value of atmospheric heating at the surface is also reported by Ganguly and Jayaraman (2006) for Ahmadabad an urban location

in western India. In the present study, it has to be emphasized that the heating rate is only theoretical, static and one dimensional estimate and it is attributed to the absorption of shortwave radiation only. Further details should consider the long wave part as well as the boundary layer processes. Based on the aircraft measurements, a similar result is also reported by Tripathi et al. (2007). They have studied the heating rate profiles for forenoon and afternoon period of the day and showed that the heating rate profile for the forenoon period is increasing with height with a first peak of 2.1 K day^{-1} at 300 m altitude and a secondary peak of 1.75 K day^{-1} at 1200 m altitude, whereas the afternoon profile shows a steady increase of heating rate with a maximum of 1.82 K day^{-1} at 1200 m.

3.4. Absorption aerosol optical depth and absorption Ångström exponent

Following the Bergstrom et al. (2007) and Russell et al. (2010), the spectral absorption aerosol optical depths (AAODs) are obtained as

$$\mathrm{AAOD}(\lambda) = [1-\mathrm{SSA}(\lambda)]\mathrm{AOD}(\lambda) \quad (4)$$

where λ is the wavelength. This technique is well applied in the clear sky conditions. The spectral variation of AAOD shows a relatively smooth decrease with wavelength and can be expressed with power law wavelength dependence. Using the Ångström power law of the form $\mathrm{AAOD}(\lambda) = K\lambda^{-\mathrm{AAE}}$, where AAE is Absorption Ångström exponent (defined as the negative of the slope of a log–log plot of the AAOD versus wavelength). The value of AAE in the wavelength range (0.380–1.020 μm) is estimated by fitting the linear least square fit on log–log scale. The value of AAE close to 1 represents the theoretical AAE value of BC aerosols as suggested by earlier papers (Bergstrom et al., 2007; Russell et al., 2010). AAE values and their standard error at three different altitudes are given in Table 5. From, Table 5 it clearly indicates that the aerosol absorption over this location is dominated by mixed aerosols as suggested in earlier papers (Bergstrom et al., 2007; Russell et al., 2010). The AAE value less than 1 is also obtained (Table 5). A similar value of AAE < 1 is also reported by many investigators (Bergstrom et al., 2007; Gyawali et al., 2009; Russell et al., 2010; and reference cited therein). This could be attributed due to the coating of black carbon with either absorbing or non-absorbing aerosols (Gyawali et al., 2009), which is further studied by Lack and Cappa (2010). Further researches are needed to understand the aerosol absorption and AAE for which the simultaneous observations at high altitude site with those in nearby valley (below the mountain peak) are essential.

4. Conclusions

The main conclusions of our studies are as follows:

1. Spectral aerosol optical depth decreases with increase in altitude and vise versa. During winter season the aerosols below 1000 m contribute to a major fraction of columnar aerosol optical depths.
2. Black carbon mass concentration and number concentration of composite aerosols near surface, both decreases as the altitude increases.
3. The aerosol mixing height generally lies in the range between 1000 and 1500 m altitudes, above which the particle concentrations are slowly varying as a function of altitude.
4. The Ångström wavelength exponent (α) retrieved from the *AOD* spectra shows the dominance of accumulation mode aerosols in the well-mixed region, where the abundance decreases with altitude.
5. The number size distribution of columnar as well as near surface revealed the bimodal (a combination of power law and unimodal log normal distribution) distributions in nature. Also the accumulation mode aerosol contributes as much as 90% to the total aerosol number concentration for both in column and surface.
6. The comparison of forcing efficiency at Haldwani and 1000 m shows that the forcing efficiency decreases as we go uphills, showing that the aerosol types are different at higher altitudes, from the more polluted one at lower altitude (Haldwani).
7. The heating at the surface level are found to be highest and decreases sharply with increase in altitude. The observed atmospheric heating is mainly caused by the domination of absorbing aerosols by virtue of the incomplete combustion of fossil fuel combustions and biomass burning activities at nearby the observational site. Also the persistence of the high BC concentration over the study region would have significant impact on the regional climate forcing.
8. The absorption Ångström exponent (AAE) obtained from the AAOD spectra shows the aerosol absorption over the site is dominated by mixed aerosols.

Acknowledgements

This work is supported by the Indian Space Research Organization under the Geosphere–Biosphere Programme (ISRO-GBP). Author U.C. Dumka thanks Dr. P. Pant, Dr. Manish Naja and Dr. N. Singh for fruitful discussions during the data analysis.

References

Ångström, A., 1961. Techniques of determining the turbidity of the atmosphere. Tellus 13, 214–223.
Ansmann, A., Althausen, D., Wandinger, U., Franke, K., Müller, D., Wagner, F., Heintzenberg, J., 2000. Vertical profiling of the Indian aerosol plume with six-wavelength lidar during INDOEX: a first case study. Geophys. Res. Lett. 27 (7), 963–966. doi:10.1029/1999GL010902.
Arnott, P.W., Hamasha, K., Moosmller, H., Sheridan, P.J., Ogren, J.A., 2005. Towards aerosol light-absorption measurements with a 7-wavelength aethalometer: evaluation with a photoacoustic instrument and 3-wavelength nephelometer. Aerosol. Sci. Technol. 39 (1), 17–29.
Babu, S.S., Sreekanth, V., Moorthy, K.K., Mohan, M., Kirankumar, N.V.P., Subrahamanyam, D.B., Gogoi, M.M., Kompalli, S.K., Beegum, N., Chaubey, J.P., Kumar, V.H.A., Manchanda, R.K., 2011. Vertical profiles of aerosol black carbon in the atmospheric boundary layer over a tropical coastal station: perturbations during an annular solar eclipse. Atmos. Res. 99, 471–478.
Babu, S.S., Moorthy, K.K., Satheesh, S.K., 2004. Aerosol black carbon over Arabian Sea during intermonsoon and summer monsoon seasons. Geophys. Res. Lett. 31, L06104. doi:10.1029/2003GL018716.
Babu, S.S., Satheesh, S.K., Moorthy, K.K., 2002. Aerosol radiative forcing due to enhanced black carbon at an urban site in India. Geophys. Res. Lett. 29 (18), 1880. doi:10.1029/2002GL015826.
Badarinath, K.V.S., Kharol, S.K., Kaskaoutis, D.G., Kambezidis, H.D., 2007. Influence of atmospheric aerosols on solar spectral irradiance in an urban area. J. Atmos. Sol.-Terr. Phys. 69, 589–599.
Bergstrom, R.W., Pilewskie, P., Russell, P.B., Redemann, J., Bond, T.C., Quinn, P.K., Sierau, B., 2007. Spectral absorption properties of atmospheric aerosols. Atmos. Chem. Phys. 7, 5937–5943.
Bodhaine, B.A., 1995. Aerosol absorption measurements at Barrow, Mauna Loa and the South Pole. J. Geophys. Res. 100, 8967–8975.
Cheng, T., Han, Z., Zhang, R., Du, H., Jia, X., Wang, J., Yao, J., 2010. Black carbon in a continental semiarid area of northeast China and its possible sources of fire emission. J. Geophys. Res. 115, D23204. doi:10.1029/2009JD013523.
Chinnam, N., Dey, S., Tripathi, S.N., Sharma, M., 2006. Dust events in Kanpur, northern India: chemical evidence for source and implications to radiative forcing. Geophys. Res. Lett. 33, L08803. doi:10.1029/2005GL025278.
Chung, C.E., Ramanathan, V., Kim, D., Podgorny, I.A., 2005. Global anthropogenic aerosol direct forcing derived from satellite and ground-based observations. J. Geophys. Res. 110, D24207. doi:10.1029/2005JD006356.
Conant, W.C., et al., 2003. A model for the radiative forcing during ACE—Asia derived from CIRPAS Twin Otter and R/V Ronald H. Brown data and

comparison with observations. J. Geophys. Res. 108 (D23), 8661. doi:10.1029/2002JD003260.
Corrigan, C.E., Ramanathan, V., Schauer, J.J., 2006. Impact of monsoon transitions on the physical and optical properties of aerosols. J. Geophys. Res. 111, D18208. doi:10.1029/2005JD006370.
Devara, P.C.S., Raj, P.E., Pandithurai, G., 1995. Aerosol-profile measurements in the lower troposphere with four-wavelength bistatic argon-ion lidar. Appl. Opt. 34 (21), 4416–4425.
Dey, S., Tripathi, S.N., 2008. Aerosol direct radiative effects over Kanpur in the Indo-Gangetic basin, northern India: long-term (2001–2005) observations and implications to regional climate. J. Geophys. Res. 113, D04212. doi:10.1029/2007JD009029.
Dumka, U.C., Moorthy, K.K., Kumar, R., Hegde, P., Sagar, R., Pant, P., Singh, N., Babu, S.S., 2010. Characteristics of aerosol black carbon mass concentration over a high altitude location in the central Himalayas from multi-year measurements. Atmos. Res. 96, 510–521.
Dumka, U.C., Sagar, R., Pant, P., 2009. Retrieval of columnar aerosol size distributions from spectral attenuation measurements over central Himalayas. Aerosol Air Qual. Res. 9, 344–351.
Dumka, U.C., Moorthy, K. Krishna, Satheesh, S.K., Sagar, Ram, Pant, P., 2008. Short-period modulations in aerosol optical depths over the central Himalayas: role of mesoscale processes. J. Appl. Meteorol. Climatol. 47, 1467–1475. doi:10.1175/2007JAMC16381.
Eck, T.F., Holben, B.N., Ward, D.E., Mukelabai, M.M., Dubovik, O., Smirnov, A., Schafer, J.S., Hsu, N.C., Piketh, S.J., Queface, A., Roux, J. Le., Swap, R.J., Slutsker, I., 2003. Variability of biomass burning aerosol optical characteristics in southern Africa during the SAFARI 2000 dry season campaign and a comparison of single scattering albedo estimates from radiometric measurements. J. Geophys. Res. 108 (D13), 8477. doi:10.1029/2002JD002321.
Favez, O., Alfaro, S.C., Sciare, J., Cachier, H., Abdelwahab, M.M., 2009. Ambient measurements of light-absorption by agricultural waste burning organic aerosols. Aerosol Sci. 40, 613–620.
Flamant, C., Pelon, J., Chazette, P., Trouillet, V., Quinn, P.K., Frouin, R., Bruneau, D., Leon, J.-F., Bates, T., Johnson, J., Livingston, J., 2000. Airborne Lidar measurements of aerosol spatial distribution and optical properties over the Atlantic Ocean during an European pollution outbreak of ACE-2. Tellus 52B, 662–677.
Gadhavi, H., Jayaraman, A., 2006. Airborne Lidar study of the vertical distribution of aerosols over Hyderabad, an urban site in central India, and its implication for radiative forcing calculations. Ann. Geophys. 24, 2461–2470.
Ganguly, D., Ginoux, P., Ramaswamy, V., Dubovik, O., Welton, J., Reid, A.E., Holben, B.N., 2009. Inferring the composition and concentration of aerosols by combining AERONET and MPLNET data: comparison with other measurements and utilization to evaluate GCM output. J. Geophys. Res. 114, D16203. doi:10.1029/2009JD011895.
Ganguly, D., Jayaraman, A., 2006. Physical and optical properties of aerosols over an urban location in western India: implications for shortwave radiative forcing. J. Geophys. Res. 111, D24207. doi:10.1029/2006JD007393.
Ganguly, D., Jayaraman, A., Gadhavi, H., 2006. Physical and optical properties of aerosols over an urban location in western India: seasonal variabilities. J. Geophys. Res. 111, D24206. doi:10.1029/2006JD007392.
Gogoi, M.M., Moorthy, K.K., Babu, S.S., Bhunyan, P.K., 2009. Climatology of columnar aerosol properties and the influence of synoptic conditions—first time results from the northeastern region of India. J. Geophys. Res. 114, D08202.
Gyawali, M., Arnott, W.P., Lewis, K., Moosmüller, H., 2009. In situ aerosol optics in Reno, NV, USA during and after the summer 2008 California wildfires and the influence of absorbing and non-absorbing organic coatings on spectral light absorption. Atmos. Chem. Phys. 9, 8007–8015.
Hansen, A.D.A., 1996. Magee Scientific Aethalometer User's Guide. Magee Scientific Co., Berkeley, CA, 56 pp.
Haywood, J.M., Ramaswamy, V., 1998. Global sensitivity studies of the direct forcing due to anthropogenic sulfate and black carbon aerosols. J. Geophys. Res. 103, 6043–6058.
Hess, M., Koepke, P., Schultz, I., 1998. Optical properties of aerosols and clouds: the software package OPAC. Bull. Am. Meteorol. Soc. 79, 831–844.
Ichoku, Charles, Levy, Robert, Kaufman, Yoram J., et al., 2002. Analysis of the performance characteristics of the five-channel Microtops II Sun Photometer for measuring aerosol optical thickness and perceptible water vapor. J. Geophys. Res. 107, D13. doi:10.1029/2001JD001302.
Intergovernmental Panel on Climate Change, 2007. Climate Change, 2007: the Scientific Basis. In: Houghton, J.T., et al. (Ed.), Contribution of Working Group I to the Third Assessment Report of the Intergovernmental Panel on Climate Change. Cambridge University Press, New York.
Jayaraman, A., Ramachandran, S., Acharya, Y.B., Subbaraya, B.H., 1995. Pinatubo volcanic aerosol layer decay observed at Ahmedabad (23°N) India using Nd:YAG backscatter lidar. J. Geophys. Res. 100, 23 209–23 214.
Kaskaoutis, D.G., Kambezidis, H.D., Adamopoulos, A.D., Kassomenos, P.A., 2006. On the determination of aerosols using the Ångström exponent in the Athens area. J. Atmos. Sol.-Terr. Phys. 68, 2143–2147.
Kim, Sang-Woo, Yoon, Soon-Chang, Jefferson, Anne, Won, Jae-Gwang, Dutton, Ellsworth G., Ogren, John A., Anderson, Theodore L., 2004. Observation of enhanced water vapor in Asian dust layer and its effect on atmospheric radiative heating rates. Geophys. Res. Lett. 31 (18), L18113. doi:10.1029/2004GL020024.
King, M.D., 1982. Sensitivity of constrained linear inversion to the selection of Lagrange multiplier. J. Atmos. Sci. 39, 1356–1369.
King, M.D., Byrne, D.L., Herman, B.M., Reagan, J.A., 1978. Aerosol size distributions obtained by inversion of spectral optical depth measurements. J. Atmos. Sci. 35, 2153–2167.
Lack, D.A., Cappa, C.D., 2010. Impact of brown and clear carbon on light absorption enhancement, single scatter albedo and absorption wavelength dependence of black carbon. Atmos. Chem. Phys. 10, 4207–4220.
Lesins, G., Bourdages, L., Duck, T.J., Drummond, T.J., Eloranta, E.W., Walden, V.P., 2009. Large surface radiative forcing from topographic blowing snow residuals measured in the High Arctic at Eureka. Atmos. Chem. Phys. 9, 1847–1862.
Li, Zhanqing, Lee, Kwon-Ho, Wang, Tuesi, Xin, Jinyuan, Hao, Wei-Min, 2010. First observation-based estimates of cloud-free aerosol radiative forcing across China. J. Geophys Res. 115, D00K18. doi:10.1029/2009JD013306.
Liou, K.N., 1980. An Introduction to Atmospheric Radiation. Harcourt Brace 593 Jovanovich, New York, 392 pp.
Ma, Jianzhong, Chen, Yue, Wang, Wei, Yan, Peng, Liu, Hongjie, Yang, Suying, Hu, Zhijin, Lelieveld, Jos, 2010. Strong air pollution causes widespread haze-clouds over China. J. Geophys. Res. 115, D18204. doi:10.1029/2009JD013065.
McComiskey, A., Schwartz, S.E., Schmid, B., Guan, H., Lewis, E.R., Ricchiazzi, P., Ogren, J.A., 2008. Direct aerosol forcing: calculation from observables and sensitivities to inputs. J. Geophys. Res. 113 (D9), D09202. doi:10.1029/2007JD009170.
McGill, M.J., Hlavka, D.L., Hart, W.D., Welton, E.J., Campbell, J.R., 2003. Airborne Lidar measurements of aerosol optical properties during SAFARI-2000. J. Geophys. Res. 108 (D13), 8493. doi:10.1029/2002JD002370.
Moorthy, K.K., Babu, S.S., Satheesh, S.K., 2005. Aerosol characteristics and radiative impacts over the Arabian Sea during the intermonsoon season: results from ARMEX field campaign. J. Atmos. Sci. 62, 192–206.
Moorthy, K.K., Nair, V.S., Babu, S.S., Satheesh, S.K., 2009. Spatial and vertical heterogeneities in aerosol properties over oceanic regions around India: implications for radiative forcing. Q. J. R. Meteorol. Soc. doi:10.1002/qj.525.
Moorthy, K.K., Babu, S.S., Sunilkumar, S.V., Gupta, P.K., Gera, B.S., 2004. Altitude profiles of aerosol BC derived from aircraft measurements over an inland urban location in India. Geophys. Res. Lett. 31, L22103. doi:10.1029/2004GL021336.
Moorthy, K.K., Satheesh, S.K., Murthy, B.V.K., 1997. Investigations of marine aerosols over the tropical Indian Ocean. J. Geophys. Res. 102 (D15), 18827–18842. doi:10.1029/97JD01121.
Morys, M., Mims III, F.M., Hagerup, S., Anderson, S.E., Baker, A., Kia, J., Walkup, T., 2001. Design, calibration and performance of MICROTOPS II hand-held ozone monitor and Sun Photometer. J. Geophys. Res. 106 (D13), 14,573–14,582.
Müller, D., Franke, K., Wagner, F., Althausen, D., Ansmann, A., Heintzenberg, J., 2001. Vertical profiling of optical and physical particle properties over the tropical Indian Ocean with six-wavelength lidar. 1. Seasonal cycle. J. Geophys. Res. 106 (D22), 28567–28575.
Niranjan, K., Sreekanth, V., Madhavan, B.L., Moorthy, K. Krishna, 2007. Aerosol physical properties and radiative forcing at the outflow region from the Indo-Gangetic plains during typical clear and hazy periods of wintertime. Geophys. Res. Lett. 34, L19805. doi:10.1029/2007GL031224.
Pandithurai, G., Pinker, R.T., Takamura, T., Devara, P.C.S., 2004. Aerosol radiative forcing over a tropical urban site in India. Geophys. Res. Lett. 31, L12107. doi:10.1029/2004GL019702.
Pant, P., Hegde, P., Dumka, U.C., Sagar, Ram, Satheesh, S.K., Moorthy, K. Krishna, Auromeet, Saha, Srivastava, M.K., 2006. Aerosol characteristics at a high altitude location in central Himalayas: Optical properties and radiative forcing. J. Geophys. Res. 111, D17206. doi:10.1029/2005JD006768.
Parameswaran, K., Rajan, R., Vijayakumar, G., Rajeev, K., Moorthy, K.K., Nair, P.R., Satheesh, S.K., 1998. Seasonal and long term variations of aerosol content in the atmospheric mixing region at a tropical station on the Arabian Sea-coast. J. Atmos. Sol.-Terr. Phys. 60 (1), 17–25.
Pathak, B., Kalita, G., Bhuyan, K., Bhuyan, P.K., Moorthy, K.K., 2010. Aerosol temporal characteristics and its impact on shortwave radiative forcing at a location in the northeast of India. J. Geophys. Res. 115, D19204. doi:10.1029/2009JD013462.
Pelon, J., Flamant, C., Chazette, P., Leon, J.-F., Tanŕe, D., Sicard, M., Satheesh, S.K., 2002. Characterization of aerosol spatial distribution and optical properties over the Indian Ocean from air-borne LIDAR and radiometry during INDOEX-99. J. Geophys. Res. 107 (D19), 8029. doi:10.1029/2001JD000402.
Pilinis, C., Pandis, S.N., Seinfeld, J.H., 1995. Sensitivity of direct climate forcing of atmospheric aerosols to aerosol size and composition. J. Geophys. Res. 100 (D9), 18,739–18,754.
Podgorny, I.A., Conant, W., Ramanathan, V., Satheesh, S.K., 2000. Aerosol modulation of atmospheric and surface solar heating over the tropical Indian Ocean. Tellus Ser. B 52, 1–12.
Porter, John N., Miller, Mark, Pietras, Chritophe, Craig, Motell, 2001. Ship-based Sun Photometer measurements using Microtops Sun Photometers. J. Atmos. Oceanic Technol. 18 (5), 765–774.
Ramachandran, S., Kedia, Sumita, 2010. Black carbon aerosols over an urban region: radiative forcing and climate impact. J. Geophys. Res. 115, D10202. doi:10.1029/2009JD013560.
Ramachandran, S., Rajesh, T.A., 2007. Black carbon aerosol mass concentrations over Ahmadabad, an urban location in western India: comparison with urban sites in Asia, Europe, Canada, and the United States. J. Geophys. Res. 112, D06211. doi:10.1029/2006JD007488.
Ramana, M.V., Ramanathan, V., Podgorny, I.A., Pradhan Bidya, B., Basanta, Shrestha, 2004. The direct observations of large aerosol radiative forcing in the Himalayan region. Geophys. Res. Lett. 31, L05111. doi:10.1029/2003GL018824.

Ricchiazzi, P., Yang, S., Gautier, C., Sowle, D., 1998. SBDART: a research and teaching software tool for plane-parallel radiative transfer in the earth's atmosphere. Bull. Am. Meteorol. Soc. 79, 2101–2114.

Russell, P.B., Bergstrom, R.W., Shinozuka, Y., Clarke, A.D., DeCarlo, P.F., Jimenez, J.L., Livingston, J.M., Redemann, J., Dubovik, O., Strawa, A., 2010. Absorption Angstrom exponent in AERONET and related data as an indicator of aerosol composition. Atmos. Chem. Phys. 10, 1155–1169.

Russell, P.B., Livingston, J.M., Dutton, E.G., Pueschel, R.F., Reagon, J.A., Defoor, T.E., Box, M.A., Allen, D., Pilewskie, P., Herman, B.M., Kinnie, S.A., Hofmann, D.J., 1993. Pinatubo and pre-pinatubo optical depth spectra: Mauna Loa measurements, comparisons, inferred particle size distribution, radiative effects and relationship to Lidar data. J. Geophys. Res. 98, 22969–22985.

Saha, A., Moorthy, K.K., 2004. Impact of precipitation on aerosol spectral optical depth and retrieved size distributions: a case study. J. Appl. Meteorol. 42, 902–914.

Sasano, Y., Shimizu, H., Sugimoto, N., Matsui, I., Takeuchi, N., Okuda, M., 1982. Diurnal variation of the atmospheric planetary boundary layer observed by a computer controlled laser radar. J. Meteorol. Soc. Jpn. 58, 143–148.

Satheesh, S.K., Moorthy, K.K., 1997. Aerosol characteristics over coastal regions of the Arabian Sea. Tellus Ser. B 49, 417–428.

Satheesh, S.K., 2002. Aerosol radiative forcing over land: effect of surface and cloud reflection. Ann. Geophys. 20 (12), 2105–2109.

Satheesh, S.K., Vinoj, V., Moorthy, K. Krishna, 2006. Vertical distribution of aerosols over an urban continental site in India inferred using a micro-pulse lidar. Geophys. Res. Lett. 33, L20816. doi:10.1029/2006GL027729.

Satheesh, S.K., Ramanathan, V., 2000. Large differences in the tropical aerosol forcing at the top of the atmosphere and Earth's surface. Nature 405, 60–63.

Satheesh, S.K., Srinivasan, J., 2006. A method to estimate aerosol radiative forcing from spectral optical depths. J. Atmos. Sci. 63, 1082–1092.

Satheesh, S.K., Ramanathan, V., Li-Jones, X., Lobert, J.M., Podgorny, I.A., Prospero, J.M., Holben, B.N., Loeb, G.N., 1999. A model for the natural and anthropogenic aerosols over the tropical Indian Ocean derived from Indian Ocean Experiment data. J. Geophys. Res. 104, 27421–27440.

Satheesh, S.K., Ramanathan, V., Holben, B.N., Moorthy, K.K., Loeb, N.G., Maring, H., Prospero, J.M., Savoie, D., 2002. Chemical, microphysical and radiative effects of Indian Ocean aerosols. J. Geophys. Res. 107, 4725. doi:10.1029/2002JD002462.

Satheesh, S.K., Srinivasan, J., 2002. Enhanced aerosol loading over Arabian Sea during pre-monsoon season: Natural or anthropogenic? Geophys. Res. Lett. 29 (18), 1874. doi:10.1029/2002GL015687.

Sheridan, P.J., et al., 2005. The Reno Aerosol Optics Study: an evaluation of aerosol absorption measurement methods. Aerosol. Sci. Technol. 39, 1–16.

Tripathi, S.N., Srivastava Atul, K., Sagnik, Dey, Satheesh, S.K., Krishnamoorthy, K., 2007. The vertical profile of atmospheric heating rate of black carbon aerosols at Kanpur in Northern India. Atmos. Environ. 41, 6909–6915.

Tripathi, S.N., Dey, S., Tare, V., Satheesh, S.K., Shyam, Lal, Venkataramani, S., 2005a. Enhanced layer of black carbon in a north Indian industrial city. Geophys. Res. Lett. 32, L12802. doi:10.1029/2005GL022564.

Tripathi, S.N., Dey, S., Tare, V., Satheesh, S.K., 2005b. Aerosol black carbon radiative forcing at an industrial city in northern India. Geophys. Res. Lett. 32, L08802. doi:10.1029/2005GL022515.

Vinoj, V., Satheesh, S.K., 2003. Measurements of aerosol optical depths over Arabian Sea during summer monsoon season. Geophys. Res. Lett. 30 (5), 1263. doi:10.1029/2002GL016664.

Vinoj, V., Babu, S.S., Satheesh, S.K., Moorthy, K.K., Kaufman, Y.J., 2004. Radiative forcing by aerosols over the Bay of Bengal region derived from shipborne, island-based, and satellite (Moderate-Resolution Imaging Spectroradiometer) observations. J. Geophys. Res. 109, D05203. doi:10.1029/2003JD004329.

Vinoj, V., Satheesh, S.K., Moorthy, K.K., 2010. Optical, radiative, and source characteristics of aerosols at Minicoy, a remote island in the southern Arabian Sea. J. Geophys. Res. 115, D01201. doi:10.1029/2009JD011810.

Weingartner, E., Saathoff, H., Schnaiter, M., Streit, N., Bitnar, B., Baltensperger, U., 2003. Absorption of light by soot particles: determination of the absorption coefficient by means of aethalometers. J. Aerosol. Sci. 34, 1445–1463.